Structural Engineering and Mechanics, *Vol. 68, No. 1 (2018) 1-15*
DOI: https://doi.org/10.12989/sem.2018.68.1.001

Hydrodynamic analysis of floating structures with baffled ARTs

San Kim[1a] and Kang-Heon Lee[*2]

[1]*Department of Mechanical Engineering, Korean Advanced Institute for Science and Technology, 291 Daehak-ro, Yuseong-gu, Daejeon 34141, Republic of Korea*
[2]*Korea Atomic Energy Research Institute, 111 Daehak-ro 989 beon-gil, Yuseong-gu, Daejeon 34057, Republic of Korea*

(Received July 16, 2018, Revised August 28, 2018, Accepted September 6, 2018)

Abstract. In ocean industry, free surface type ART (Anti Roll tank) system has been widely used to suppress the roll motion of floating structures. In those, various obstacles have been devised to obtain the sufficient damping and to enhance the controllability of freely rushing water inside the tank. Most of previous researches have paid on the development of simple mathematical formula for coupled ship-ARTs analysis although other numerical and experimental approaches exist. Little attention has been focused on the use of 3D panel method for preliminary design of free surface type ART despite its advantages in computational time and general capacity for hydrodynamic damping estimation.

This study aims at developing a potential theory based hydrodynamic code for the analysis of floating structure with baffled ARTs. The sloshing in baffled tanks is modeled through the linear potential theory with FE discretization and it coupled with hydrodynamic equations of floating structures discretized by BEM and FEM, resulting in direct coupled FE-BE formulation. The general capacity of proposed formulation is emphasized through the coupled hydrodynamic analysis of floating structure and sloshing inside baffled ARTs. In addition, the numerical methods for natural sloshing frequency tuning and estimation of hydrodynamic damping ratio of liquid sloshing in baffled tanks undergoing wave exiting loads are developed through the proposed formulation. In numerical examples, effects of natural frequency tuning and baffle ratios on the maximum and significant roll motions are investigated.

Keywords: anti roll tank; baffle; linear potential theory; hydrodynamic damping; hydrodynamic analysis; fluid-structure interaction

1. Introduction

When the natural roll frequency of ships (i.e., ongoing vessels, pipe-laying ships and drill ships) and offshore platforms coincide with the peak frequency of wave energy spectrum, it could bring out the dramatic increase of roll motion. It is well known as synchronous rolling and it should be suppressed (Sellars and Martin 1992, Cho *et al*. 2012). After the considerable work were made by Froude (1861) and Watt (1883, 1885), anti-roll tank (ART) system has been devised to stabilize the roll motion by increasing the damping in roll. For decades, various ART systems have been suggested (i.e., U-type, n-type, free surface type) and the comprehensive review on the ARTs were recently summarized in the reference (Moaleji and Greig 2007). There have also been studies to reduce motion by applying various types of damper to on and offshore structures (Jeon *et al*. 2013, Bhosale *et al*. 2017, Rahman *et al*. 2017).

In following, the free surface type ART is considered. The important feature is that it can change its state (i.e., free surface correction factor, natural sloshing frequency) by changing the water depth within the tanks (Faltinsen and Timokha 2009) whereas this feature not so readily achieved in U-tanks, n-tanks, and other types. Many researchers (Van and Vugts 1966, Goodrich 1969, Lewison 1976) have numerically studied the free surface type without consideration of obstacles and they emphasized the effects of location, size, mass, damping, and natural frequency tuning of tanks on the global roll motion of ships.

The essential issue that should be considered in free surface type is the control of water which rushes freely from side to side in the tank since it could threat the safety of tanks by bringing out the unstable motion of the ship in rough sea. Moreover, these can induce the high energy spectrum for roll motion when one of the two peak frequencies of roll RAO is close to the peak frequency of the wave energy spectrum. Accordingly, the baffle and other obstacles have been devised and installed inside tanks.

When the baffle is considered, the effects of additional hydrodynamic damping and the natural sloshing frequency change induced by baffle should be carefully taken into the preliminary design of ARTs in line with design parameters mentioned above. Lee and Vassalos (1996) experimentally showed the performance characteristics of ARTs with various screens. Also, Francescutto *et al*. (1999) described the effect of baffled ARTs by using the Reynolds averaged Navier-Stokes equation based mathematical model and Kim (2002) developed the fully coupled numerical method for the analysis of ship motion and nonlinear sloshing in ARTs with internal pillars. Also, after Souto and Gonzalez (2001) and Iglesias *et al.* (2004), many researchers have tried to simulate the nonlinear sloshing using the SPH (Smoothed

*Corresponding author, Researcher
E-mail: khlee72@kaeri.re.kr
[a]Ph.D. Student

http://www.techno-press.com/journals/sem&subpage=7
ISSN: 1225-4568 (Print), 1598-6217 (Online)

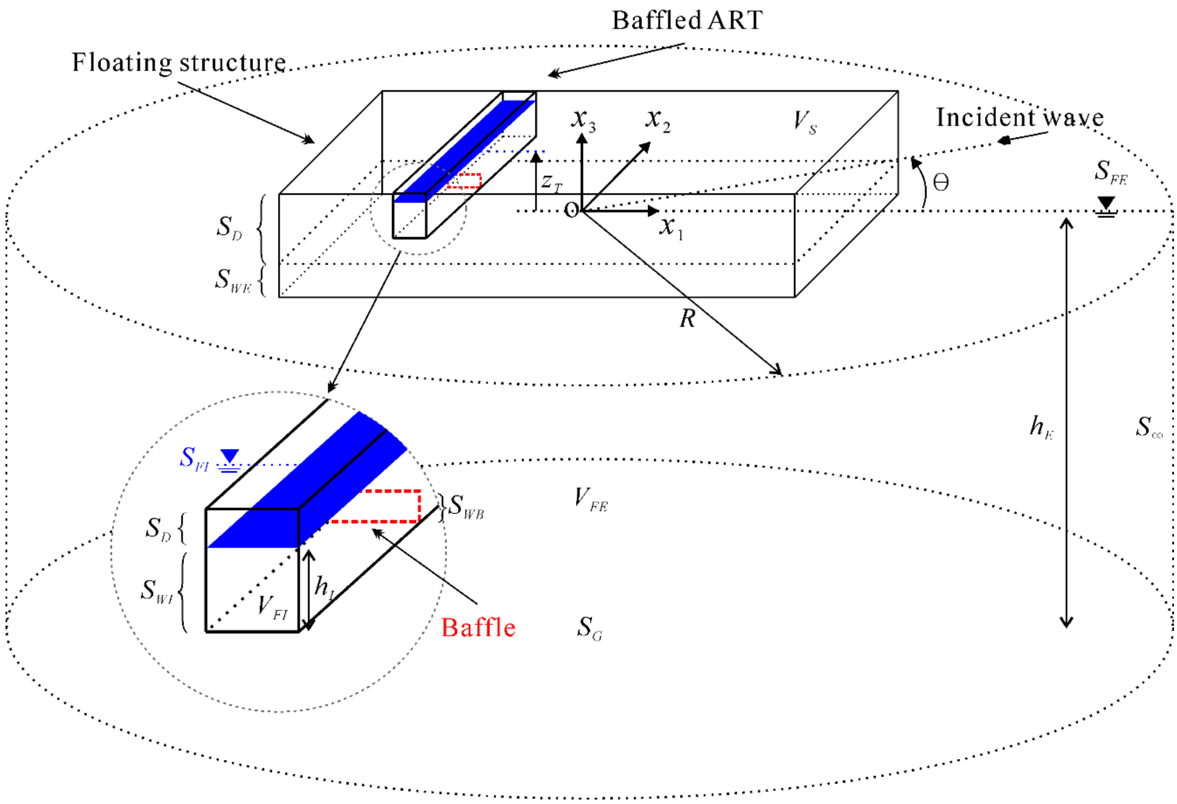

Fig. 1 Problem description of a floating structure interacting with baffled ARTs in an incident water wave

Particle Hydrodynamics) method. Most of their effort has been concentrated on the nonlinear sloshing simulation and their validation with experiments.

Recently, various 3D panel programs (i.e., WAMIT (Lee and Newman 2006) and Hydrostar (Bureau 2007)) have been developed for the hydrodynamic analysis of floating structures and have been extended to the analysis of fully coupled ship and sloshing motion. Because of potential code requires the relatively small computational time than Navier-Stokes solver; this can be a useful method in preliminary design of ARTs which requires series of hydrodynamic analyses. However, sloshing in baffled tanks has not been considered in 3D panel method so far. In addition, the numerical procedure for hydrodynamic damping estimation of liquid sloshing in baffled tank undergoing wave exciting loads has not been developed even though its general capacity of linear sloshing for hydrodynamic damping estimation were researched and verified by many researchers (Isaacson and Premasiri 2001, Maleki and Ziyaeifar 2008, Goundarzi and Sabbagh-Yazdi 2012). Therefore, the numerical model should be developed for the use of 3D panel programs in preliminary design of ARTs with baffles.

In this study, the direct coupled formulation which has been developed by many researchers (Taylor 2007, Khabakhpasheva and Korobkin 2002, Wang and Meylan 2004, Kim *et al.* 2013) is employed and extended to sea-keeping problem with baffled ARTs. The linear potential theory is used for the modeling of external gravity waves and linear sloshing in baffled tank whereas the continuum mechanics is applied to the modeling of floating structures. The finite element method (FEM) is employed not only for the discretization of the floating structure, ARTs, and baffles within tanks but also for the internal fluid whereas the boundary element method (BEM) is applied to discretize the integral equations of external fluids. The general capacity of proposed formulation is demonstrated through the hydrodynamic analysis of floating structure with baffled ART system. Moreover, the eigenvalue problem of sloshing in baffled tank and a numerical procedure for hydrodynamic damping ratio estimation of liquid sloshing in baffled tanks are developed by extending the proposed formulation.

In validation section, the proposed numerical method is verified through the various numerical tests. Then, in numerical examples, the series of hydrodynamic analysis are conducted to emphasize the effects of natural frequency tuning and baffle ratio on the maximum and significant roll motions. In addition, numerical procedures for natural frequency tuning and hydrodynamic damping estimation are demonstrated in detail.

2. Theoretical background

In this section, the mathematical formulation for the hydrodynamic analysis of floating structure with baffled ART is developed in frequency domain. The equation of motion for floating structure is obtained through the continuum mechanics and the equations for external and internal fluids are derived using the linear potential theory. The full derivation of the floating structure and the external fluid parts can be found in the literatures (Kim *et al.* 2013).

As shown in Fig. 1, a fluid-structure interaction problem among an incident water wave, floating structures and sloshing within the baffled ARTs is considered and a fixed Cartesian coordinate system (x_1, x_2, x_3) is introduced on the external free surface of calm water. The subscripts *i* and *j*, which vary from 1 to 3, are imposed in conjunction with the tensorial formulation and the Einstein summation convention.

In the formulation, hydrostatic and hydrodynamic equilibrium states are denoted by the left superscripts 0 and *t*. Then, the material point vectors for the floating structure in each state are then expressed by ${}^0x_i$ and ${}^tx_i$. Finally, the displacement vectors of the floating structure are defined by

$$ {}_0^t u_i = {}^t x_i - {}^0 x_i . \tag{1}$$

2.1 Governing equations for floating structures with baffled ARTs

The floating structure and tanks are assumed as a homogeneous, isotropic, and linear elastic material and the corresponding equilibrium equations at time *t* are

$$\frac{\partial\, {}^t\sigma_{ij}}{\partial\, {}^t x_j} - {}^t\rho_S g \delta_{i3} - {}^t\rho_S\, {}^t\ddot{x}_i = 0 \quad \text{in} \quad {}^tV_S , \tag{2a}$$

$${}^t\sigma_{ij}\, {}^t n_j = -\, {}^tP_E\, {}^t n_i \quad \text{on} \quad {}^tS_{WE} , \tag{2b}$$

$${}^t\sigma_{ij}\, {}^t n_j = -\, {}^tP_I\, {}^t n_i \quad \text{on} \quad {}^tS_{WI} \ \text{and} \ {}^tS_{WB} , \tag{2c}$$

$${}^t\sigma_{ij}\, {}^t n_j = 0 \quad \text{on} \quad {}^tS_D , \tag{2d}$$

where V_S is the volume of structures, the surface of floating structure S_S consists of the dry surface S_D, the external wet surface S_{WE}, the internal wet surface S_{WI}, and the baffled wet surface S_{WB}. In Eq. (2a), σ_{ij} is the Cauchy stress tensor, ρ_S is the density of the floating structure, n_i is the unit normal vector outward from the floating structure to both the internal and external fluids, δ_{ij} is the Kronecker delta, and the overdot represents the material time derivative. The total pressure fields of the external ${}^tP_E$ and internal ${}^tP_I$ fluid can be defined by using the linearized Bernoulli equations and those are

$$ {}^tP_E = -\rho_E g x_3 - j\omega\rho_E\varphi_E , \quad {}^tP_I = -\rho_I g x_{I3} - j\omega\rho_I\varphi_I \quad \text{with} \quad x_{I3} = x_3 - z_T , \tag{3}$$

in which ρ_E is the density of the external fluid, ρ_I is the density of the internal fluid, g is the gravitational acceleration, z_T is the vertical position of the internal free surface.

After applying the principle of virtual displacement at time *t* and invoking a harmonic response (${}_0^t u_i = \mathrm{Re}\left\{ u_i({}^0\mathbf{x}) e^{jwt} \right\}$; $j = \sqrt{-1}$), the following steady state equation for hydrodynamic analysis can be obtained (Lee and Lee 2016, Yoon and Lee 2017)

$$\begin{aligned} &-\omega^2 \int_{{}^0V_S} {}^0\rho_S u_i \bar{u}_i \mathrm{d}V + \int_{{}^0V_S} C_{ijkl} e_{kl}\, {}_0\bar{e}_{ij} \mathrm{d}V \\ &+ \int_{{}^0V_S} {}^0\sigma_{ij}\, {}_0^t\bar{\eta}_{ij} \mathrm{d}V - \int_{{}^0S_{WE}} \rho_E g u_3\, {}^0n_i \bar{u}_i \mathrm{d}S \\ &- \int_{{}^0S_{WE}} \rho_E g\, {}^0x_3\, {}^0n_j Q_{ij} \bar{u}_i \mathrm{d}S - \int_{{}^0S_{WE}} j\omega\, \rho_E \varphi_E\, {}^0n_i \bar{u}_i \mathrm{d}S \\ &- \int_{{}^0S_{WI} \cup {}^0S_{WB}} \rho_I g u_3\, {}^0n_i \bar{u}_i \mathrm{d}S - \int_{{}^0S_{WI} \cup {}^0S_{WB}} \rho_I g\, {}^0x_{I3}\, {}^0n_j Q_{ij} \bar{u}_i \mathrm{d}S \\ &- \int_{{}^0S_{WI} \cup {}^0S_{WB}} j\omega\, \rho_I \varphi_I\, {}^0n_i \bar{u}_i \mathrm{d}S = 0 , \end{aligned} \tag{4}$$

where

$$\begin{aligned} &{}_0^t e_{ij} = \mathrm{Re}\left\{ e_{ij}({}^0x_k) e^{jwt} \right\}, \quad {}_0^t\bar{\eta}_{ij} = \mathrm{Re}\left\{ \bar{\eta}_{ij}({}^0x_k) e^{jwt} \right\}, \\ &{}_t^0 Q_{ij} = \mathrm{Re}\left\{ Q_{ij}({}^0x_k) e^{jwt} \right\}, \quad {}^tP_{DE} = \mathrm{Re}\left\{ P_{DE}({}^0x_k) e^{jwt} \right\}, \\ &{}^tP_{DI} = \mathrm{Re}\left\{ P_{DI}({}^0x_k) e^{jwt} \right\} \quad \text{with} \end{aligned} \tag{5}$$

$$ Q_{ij} = \delta_{ij} \frac{\partial u_k}{\partial x_k} - \frac{\partial u_j}{\partial x_i} ,$$

in which $\bar{u}_i$ is the virtual displacement vector, ${}_0\bar{e}_{ij}$ and ${}_0^t\bar{\eta}_{ij}$ are the virtual linear and nonlinear strain tensors, and C_{ijkl} is the stress-strain relation tensor.

2.2 Governing equations for the external fluid

The governing equation and boundary conditions for the external fluid in steady state

$$ {}^t\varphi_E = \mathrm{Re}\left\{ \varphi_E(x_i) e^{jwt} \right\} , \tag{6a}$$

$$ \frac{\partial^2 \varphi_E}{\partial x_i \partial x_i} = 0 \quad \text{in} \quad {}^0V_{FE} , \tag{6b}$$

$$ \frac{\partial \varphi_E}{\partial x_3} = \frac{\omega^2}{g}\varphi_E \quad \text{on} \quad S_{FE}\ (x_3 = 0) , \tag{6c}$$

$$ \frac{\partial \varphi_E}{\partial x_3} = 0 \quad \text{on} \quad S_G\ (x_3 = -h_E) , \tag{6d}$$

$$ \sqrt{R}\left(\frac{\partial}{\partial R} + jk \right)\left(\varphi_E - \varphi^I \right) = 0 \quad \text{on} \quad S_\infty\ (R \to \infty) , \tag{6e}$$

$$ \frac{\partial \varphi_E}{\partial n} = j\omega u_i n_i \quad \text{on} \quad {}^0S_{WE} , \tag{6f}$$

where k is the wave number and φ^I is the velocity

Table 1 FE-BE discretization

Floating Structure (FEM)	External fluid (BEM)
$\omega^2 \int_{{}^0V_S} {}^0\rho_S u_i \bar{u}_i \mathrm{d}V = \hat{\bar{\mathbf{u}}}^T \omega^2 \mathbf{S}_M \hat{\mathbf{u}}$	$\int_{{}^0S_{WE}} \alpha\, \varphi_E \bar{\varphi} \mathrm{d}S = \hat{\bar{\varphi}}^T \mathbf{F}_M^E \hat{\varphi}_E$
$\int_{{}^0V_S} C_{ijkl} e_{kl}\, {}_0\bar{e}_{ij} \mathrm{d}V = \hat{\bar{\mathbf{u}}}^T \mathbf{S}_K \hat{\mathbf{u}}$	$\int_{{}^0S_{WE}} P.V. \int_{{}^0S_{WE}} \frac{\partial G}{\partial n_\xi} \varphi_E \mathrm{d}S_\xi\, \bar{\varphi}\, \mathrm{d}S_x = \hat{\bar{\varphi}}^T \mathbf{F}_{Gn} \hat{\varphi}_E$
$\int_{{}^0V_S} {}^0\sigma_{ij} \bar{\eta}_{ij} \mathrm{d}V = \hat{\bar{\mathbf{u}}}^T \mathbf{S}_{KN} \hat{\mathbf{u}}$	$j\omega \int_{{}^0S_{WE}} P.V. \int_{{}^0S_{WE}} G u_i n_i \mathrm{d}S_\xi\, \bar{\varphi}\, \mathrm{d}S_x = \hat{\bar{\varphi}}^T j\omega \mathbf{F}_G \hat{\mathbf{u}}$
$\int_{{}^0S_{WE}} \rho_E g u_3\, {}^0n_i \bar{u}_i \mathrm{d}S = \hat{\bar{\mathbf{u}}}^T \mathbf{S}_{HD}^E \hat{\mathbf{u}}$	$4\pi \int_{{}^0S_{WE}} \varphi^I\, \bar{\varphi}\, \mathrm{d}S = \hat{\bar{\varphi}}^T 4\pi \mathbf{R}^I$
$\int_{{}^0S_{WE}} \rho_E g\, {}^0x_3\, {}^0n_j Q_{ij} \bar{u}_i \mathrm{d}S = \hat{\bar{\mathbf{u}}}^T \mathbf{S}_{HN}^E \hat{\mathbf{u}}$	**Internal fluid (FEM)**
$\int_{{}^0S_{WE}} j\omega\, \rho_E \varphi_E\, {}^0n_i \bar{u}_i \mathrm{d}S = \hat{\bar{\mathbf{u}}}^T j\omega \mathbf{S}_D^E \hat{\varphi}_E$	$\int_{{}^0S_{FI}} \rho_I \left(\frac{\omega^2}{g}\right) \varphi_I \bar{\varphi} \mathrm{d}S = \hat{\bar{\varphi}}^T \omega^2\, \mathbf{F}_M^I \hat{\varphi}_I$
$\int_{{}^0S_{WI} \cup {}^0S_{WB}} \rho_I g u_3\, {}^0n_i \bar{u}_i \mathrm{d}S = \hat{\bar{\mathbf{u}}}^T \mathbf{S}_{HD}^I \hat{\mathbf{u}}$	$\int_{{}^0S_{FI}} \rho_I \left(\frac{j\omega\mu}{g}\right) \varphi_I \bar{\varphi} \mathrm{d}S = \hat{\bar{\varphi}}^T j\omega\, \mathbf{F}_C^I \hat{\varphi}_I$
$\int_{{}^0S_{WI} \cup {}^0S_{WB}} \rho_I g\, {}^0x_{I3}\, {}^0n_j Q_{ij} \bar{u}_i \mathrm{d}S = \hat{\bar{\mathbf{u}}}^T \mathbf{S}_{HN}^I \hat{\mathbf{u}}$	$\int_{{}^0V_{FI}} \rho_I \frac{\partial \varphi_I}{\partial x_i} \frac{\partial \bar{\varphi}}{\partial x_i} \mathrm{d}V = \hat{\bar{\varphi}}^T \mathbf{F}_K^I \hat{\varphi}_I$
$\int_{{}^0S_{WI} \cup {}^0S_{WB}} j\omega\, \rho_I \varphi_I\, {}^0n_i \bar{u}_i \mathrm{d}S = \hat{\bar{\mathbf{u}}}^T j\omega \mathbf{S}_D^I \hat{\varphi}_I$	$\int_{{}^0S_{WI} \cup {}^0S_{WB}} j\omega\, \rho_I\, u_i n_i \bar{\varphi} \mathrm{d}S = \hat{\bar{\varphi}}^T j\omega \mathbf{F}_W^I \hat{\mathbf{u}}$

potential for an incident wave, the external fluid is enveloped by the external wet surface S_{WE}, the external free surface S_{FE}, the surface S_∞ which is a circular cylinder with a sufficiently large radius R, and the flat bottom surface S_G. The external water depth h_E is measured from the flat bottom to the external free surface of calm water. It should be note that the incident regular water wave comes continuously from the positive x_1 direction with an angle θ.

Then, the corresponding boundary integral equation is

$$\begin{aligned} &-\int_{{}^0S_{WE}} P.V. \int_{{}^0S_{WE}} \left(\frac{\partial G}{\partial n_\xi} \varphi_E - j\omega G u_i n_i \right) \mathrm{d}S_\xi\, \bar{\varphi}\, \mathrm{d}S_x \\ &+ \int_{{}^0S_{WE}} \alpha\, \varphi_E \bar{\varphi} \mathrm{d}S = 4\pi \int_{{}^0S_{WE}} \varphi^I\, \bar{\varphi}\, \mathrm{d}S_x , \end{aligned} \tag{7}$$

in which $\bar{\varphi}$ is the test function, P.V. refers to the Cauchy principal value and α is the solid angle of the fluid surface measured from the spatial position x_i. In Eq. (7), the subscript ξ means that the integral is conducted with respect to the variable ξ_i, and $G(x_i;\xi_i)$ is the Green's function (Kim *et al*. 2013, Lee *et al*. 2015), which is located at position ξ_i and generated by a source potential with strength -4π and angular frequency ω.

2.3 Linear sloshing in baffled ARTs

In the steady state, the velocity potential ${}^t\varphi_I$ is governed by

$${}^t\varphi_I = \mathrm{Re}\left\{ \varphi_I(x_i) e^{jwt} \right\}, \tag{8a}$$

$$\frac{\partial^2 \varphi_I}{\partial x_i \partial x_i} = 0 \quad \text{in} \quad {}^0V_{FI}, \tag{8b}$$

$$\frac{\partial \varphi_I}{\partial x_3} + \frac{j\omega\mu}{g} \varphi_I = \frac{\omega^2}{g} \varphi_I \quad \text{on} \quad S_{FI}\ (x_3 = z_T), \tag{8c}$$

$$\frac{\partial \varphi_I}{\partial n} = j\omega\, u_i n_i \quad \text{on} \quad {}^0S_{WI} \quad \text{and} \quad {}^tS_{WB}, \tag{8d}$$

where φ_I is the velocity potential for the internal fluid. In Eq. (8c), the artificial damping μ is introduced to impose the damping effect inside tanks. The internal fluid is bounded by the internal wet surface S_{WI}, the internal free surface S_{FI}, and the baffled wet surface S_{WB}. The internal water depth h_I is measured from bottom of tank to the internal free surface at rest.

Then, the corresponding weak form of internal fluid can be obtained

$$\begin{aligned} &\int_{{}^0S_{FI}} \rho_I \left(\frac{\omega^2}{g}\right) \varphi_I \bar{\varphi} \mathrm{d}S - \int_{{}^0S_{FI}} \rho_I \left(\frac{j\omega\mu}{g}\right) \varphi_I \bar{\varphi} \mathrm{d}S \\ &- \int_{{}^0S_{WI} \cup {}^0S_{WB}} j\omega\, \rho_I\, u_i n_i \bar{\varphi} \mathrm{d}S - \int_{{}^0V_{FI}} \rho_I \frac{\partial \varphi_I}{\partial x_i} \frac{\partial \bar{\varphi}}{\partial x_i} \mathrm{d}V = 0 , \end{aligned} \tag{9}$$

in which $\bar{\varphi}$ is the test function.

3. Numerical methods

In this section, the matrix form of direct coupled equation is derived by using the FEM and BEM and the equation for rigid body hydrodynamic analysis is obtained through the mode superposition method. In addition, numerical procedures for natural sloshing frequency tuning and hydrodynamic damping estimation in baffled tanks are developed.

3.1 FE-BE discretization and rigid body hydrodynamics

The term-by-term finite element discretization of Eqs. (4), (7), and (9) are listed in Table 1. Then, the final discrete coupled equation for the hydrodynamic analysis of floating structures with baffled ARTs can then be expressed as

$$\begin{bmatrix} -\omega^2\mathbf{S}_M + \mathbf{S}_{CH} & -j\omega\mathbf{S}_D^E & -j\omega\mathbf{S}_D^I \\ j\omega\mathbf{F}_G & \mathbf{F}_M^E - \mathbf{F}_{Gn} & 0 \\ -j\omega\mathbf{F}_W^I & 0 & \omega^2\mathbf{F}_M^I - j\omega\mathbf{F}_C^I - \mathbf{F}_K^I \end{bmatrix} \begin{bmatrix} \hat{\mathbf{u}} \\ \hat{\varphi}_E \\ \hat{\varphi}_I \end{bmatrix} = \begin{bmatrix} 0 \\ 4\pi\mathbf{R}^I \\ 0 \end{bmatrix} \tag{10}$$

$$\text{with } \mathbf{S}_{CH} = \mathbf{S}_{KN} - \mathbf{S}_{HD}^E - \mathbf{S}_{HD}^I - \mathbf{S}_{HN}^E - \mathbf{S}_{HN}^I ,$$

where the this matrix $\mathbf{S}_{CH}$ is the complete hydrostatic stiffness of the floating liquid storage structure, $\hat{\mathbf{u}}$ denotes the nodal displacement vector for the floating structures, $\hat{\varphi}_E$ and $\hat{\varphi}_I$ are the nodal velocity potential vectors for the external and internal fluids, respectively.

Note that the direct coupled Eq. (10) has a general capacity for hydroelastic analysis and can be reduced to rigid body hydrodynamics through the conventional mode superposition method. In rigid body hydrodynamics, linear strain tensor in Eq. (4) is no longer interest and additional attention is required to the initial stress-related term in Eq. (4) that is

$$\int_{{}^0V_S} {}^0\sigma_{ij}\overline{\eta}_{ij}dV = \int_{{}^0S_{WE}} \rho_w g\, {}^0x_3\, {}^0n_i \frac{\partial u_k}{\partial\, {}^0x_i}\overline{u}_k dS + \int_{{}^0S_{WI}\cup {}^0S_{WB}} \rho_I g\, {}^0x_{I3}\, {}^0n_i \frac{\partial u_k}{\partial\, {}^0x_i}\overline{u}_k dS - \int_{{}^0V_S} {}^0\rho_s g \frac{\partial u_k}{\partial\, {}^0x_3}\overline{u}_k dV \cdot \tag{11}$$

The terms are also represented in matrix form as

$$\int_{{}^0S_{WE}} \rho_w g\, {}^0x_3\, {}^0n_i \frac{\partial u_k}{\partial\, {}^0x_i}\overline{u}_k dS = \hat{\overline{\mathbf{u}}}^T\mathbf{S}_{HS}^E\hat{\mathbf{u}} , \tag{12a}$$

$$\int_{{}^0S_{WI}\cup {}^0S_{WB}} \rho_I g\, {}^0x_{I3}\, {}^0n_i \frac{\partial u_k}{\partial\, {}^0x_i}\overline{u}_k dS = \hat{\overline{\mathbf{u}}}^T\mathbf{S}_{HS}^I\hat{\mathbf{u}} , \tag{12b}$$

$$\int_{{}^0V_S} {}^0\rho_s g \frac{\partial u_k}{\partial\, {}^0x_3}\overline{u}_k dV = \hat{\overline{\mathbf{u}}}^T\mathbf{S}_{HB}\hat{\mathbf{u}} . \tag{12c}$$

Finally, the equation for rigid body hydrodynamic analysis is obtained in the steady state

$$\begin{bmatrix} \boldsymbol{\psi}^{RT}\left(-\omega^2\mathbf{S}_M + j\omega\mathbf{S}_C + \mathbf{S}_{CH}^R\right)\boldsymbol{\psi}^R & -j\omega\boldsymbol{\psi}^{RT}\mathbf{S}_D^E & -j\omega\boldsymbol{\psi}^{RT}\mathbf{S}_D^I \\ j\omega\mathbf{F}_G\boldsymbol{\psi}^R & \mathbf{F}_M^E - \mathbf{F}_{Gn} & 0 \\ -j\omega\mathbf{F}_W^I\boldsymbol{\psi}^R & 0 & \omega^2\mathbf{F}_M^I - j\omega\mathbf{F}_C^I - \mathbf{F}_K^I \end{bmatrix} \begin{bmatrix} \mathbf{q}^R \\ \hat{\varphi}_E \\ \hat{\varphi}_I \end{bmatrix} = \begin{bmatrix} 0 \\ 4\pi\mathbf{R}^I \\ 0 \end{bmatrix} \tag{13}$$

$$\text{with } \mathbf{S}_{C,44} = 2\gamma\sqrt{\mathbf{S}_{M,44}\mathbf{S}_{CH,44}^R} ;$$

$\mathbf{S}_{C,ij} = 0$ for the other components; $i, j = 1,2,...,6$,

where $\mathbf{S}_C$ is the artificial viscous roll damping, γ is the system damping ratio divided by critical damping, and $\mathbf{S}_{CH}^R$ is the complete hydrostatic stiffness in rigid body analysis.

In Eq. (13), the displacement field of six rigid body motions can be represented as

$$\mathbf{u}^R = \boldsymbol{\psi}^R\mathbf{q}^R = q_1^R\psi_1^R + \cdots + q_6^R\psi_6^R , \tag{14}$$

in which $\psi_i^R (i = 1,2,...,6)$ means the nodal displacement vectors for the *i*-th rigid body mode (surge, sway, heave, roll, pitch, and yaw). The *i*-th rigid body mode can be obtained as follows

$$u_i^{R1} = q_1^R\delta_{1i} ,\ u_i^{R2} = q_2^R\delta_{2i} ,\ u_i^{R3} = q_3^R\delta_{3i} ,$$
$$u_i^{R4} = q_4^R\varepsilon_{ijk}\delta_{1j}\, {}^0x_k ,$$
$$u_i^{R5} = q_5^R\varepsilon_{ijk}\delta_{2j}\, {}^0x_k , \tag{15}$$
$$u_i^{R6} = q_6^R\varepsilon_{ijk}\delta_{3j}\, {}^0x_k \ \text{ for } \ i, j, k = 1,2,3 ,$$

where ε_{ijk} is the permutation symbol.

3.2 Natural sloshing frequency tuning in baffled ARTs

For the ART to work properly, it is necessary that the lowest natural sloshing frequency in transverse direction should be close to the natural roll frequency of the floating structure. Some prefer set these two natural frequencies equal, whereas others choose the lowest sloshing frequency to be 6-10% higher than the natural roll frequency of floating structures (Van and Vugts 1966). For example, in case of un-baffled three-dimensional rectangular tank, the natural frequency can easily found through the simple analytic form (Van and Vugts 1966)

$$\omega_{m,n}^A = \sqrt{gk_{m,n}\tanh k_{m,n}h_I} ,$$
$$k_{m,n} = \pi\sqrt{\left(\frac{m}{L_T}\right)^2 + \left(\frac{n}{W}\right)^2} \tag{16}$$
$$\text{with } m, n = 0, 1, 2, ... ;\ m + n \neq 0 ,$$

where the subscripts *m* and *n* denote the longitudinal and transverse directions and $\omega_{m,n}^A$ is the analytical solution of the sloshing natural frequencies. Then, the water depth corresponding to the first transverse natural sloshing frequency ($m = 0,\ n = 1$) can be found by

$$h_I = \frac{1}{k_{0,1}} \cdot \tanh^{-1}\left(\frac{\left(\omega_{0,1}^{A}\right)^2}{g k_{0,1}}\right). \tag{17}$$

In baffled or complex shape tank cases, the analytical approach requires the significant effort in natural sloshing frequency calculation, whereas the numerical approach is more convenient and efficient for the calculation of natural sloshing frequency in baffled or complex geometry tank cases. In this study, the natural sloshing frequency is numerically evaluated by using the terms of internal fluid parts in Eq. (13). Then, the corresponding eigenvalue problem is

$$\mathbf{F}_K^I \gamma_i = \lambda_i \mathbf{F}_M^I \gamma_i;\quad i = 1,2,\ldots,M, \tag{18}$$

in which λ_i is the eigenvalue, γ_i is the corresponding eigenvectors, M is the total degree of freedom for the Eq. (18).

Then, the water depth corresponding object natural frequency tuning condition can be found through the widely used curve fitting scheme after the natural sloshing frequencies are broadly contained with respect to various water depths.

3.3 Hydrodynamic damping estimation

When the baffle is installed inside the ART system, hydrodynamic damping should be carefully evaluated since it varies with respect to ratio, position, and numbers of baffles as well as the loading conditions. In this research, the widely used numerical approach (Isaacson and Premasiri 2001, Maleki and Ziyaeifar 2008, Goundarzi and Sabbagh-Yazdi 2012) is considered to estimate the hydrodynamic damping ratio of liquid sloshing in baffled ARTs. This approach showed good agreement with experiments and it can be extended for the numerical estimation of hydrodynamic damping ratio under the harmonic water waves.

For the hydrodynamic damping evaluation, the velocity field of internal fluid in ARTs should be obtained. In previous studies (Isaacson and Premasiri 2001, Maleki and Ziyaeifar 2008, Goundarzi and Sabbagh-Yazdi 2012), the analytic values were obtained and used since the solution can be obtained easily under the simple harmonic force and geometry. In contrast, in this study, the velocity field of internal fluid is numerically calculated by solving the Eq. (10) or Eq. (13) since the analytic solution of internal fluid is hard to obtain under the wave exciting loads. Once the velocity field of internal fluid is obtained, the hydrodynamic damping ratio can be estimated through the following procedure.

When baffles are devised in the ARTs, the flow separation effect dominates the boundary layer effect. Therefore, it can be assumed that the energy is dissipated mostly by pressure drag and the amount of drag force dF can be estimated over the baffle area, dS_{WB}

$$dF = \frac{1}{2}\rho_I C_d V_f \left|V_f\right| dS_{WB}, \tag{19}$$

where C_d is the empirical drag coefficient and V_f is the relative flow velocity against to the baffles. Strictly speaking, it is assumed that the liquid velocity field is not significantly changed by the presence of baffle and therefore the hydrodynamic damping ratio is estimated by using the potential solution of internal fluid in un-baffled ART case.

Then, the corresponding contribution to the average rate of energy dissipation D during one exited wave frequency ω is expressed by

$$D = \frac{1}{2}\rho_I \int_{\omega}\int_{S_{WB}} C_d \left|V_f^3\right| dS d\omega, \tag{20}$$

in which the drag coefficient of wall bounded baffles may be fitted (Miles 1958) by

$$C_d = 22.5\left(\frac{V_f T}{L_b}\right)^{-0.5} \quad \text{for } 1 \le \frac{V_f T}{L_b} \le 30, \tag{21}$$

where L_b is the length of baffle and T is the period of wave exciting force.

Meanwhile, the total energy of liquid oscillation can be obtained by the following relation in one wave exciting cycle

$$E = \frac{1}{4}\rho_I g \int_{S_{FI}} \eta_{a,\max}^2 dS, \tag{22}$$

where E is the maximum gravitational potential energy and $\eta_{a,\max}$ is the maximum free surface elevation during one cycle.

Finally, the additional hydrodynamic damping ratio μ_{add} can be obtained through the relation between ratio of energy dissipation rate and total energy of a system during one excited wave frequency interval

$$\mu_{add}(\omega) = \left(\frac{1}{2\omega}\right)\left(\frac{D}{E}\right). \tag{23}$$

4. Verification

The direct coupled FE-BE formulation was proposed for the hydrodynamic analysis of floating structure with baffled ARTs in the previous section. In addition, numerical methods for hydrodynamic damping estimation and natural sloshing frequency calculation in baffled tanks were introduced. For the accurate analysis, those should be verified by comparing with experimental or numerical results. Initially, the linear sloshing in baffled tank is tested through the eigenvalue analysis and the hydrodynamic damping estimation procedure is verified in simple loading condition. Finally, the fully coupled hydrodynamic code is verified.

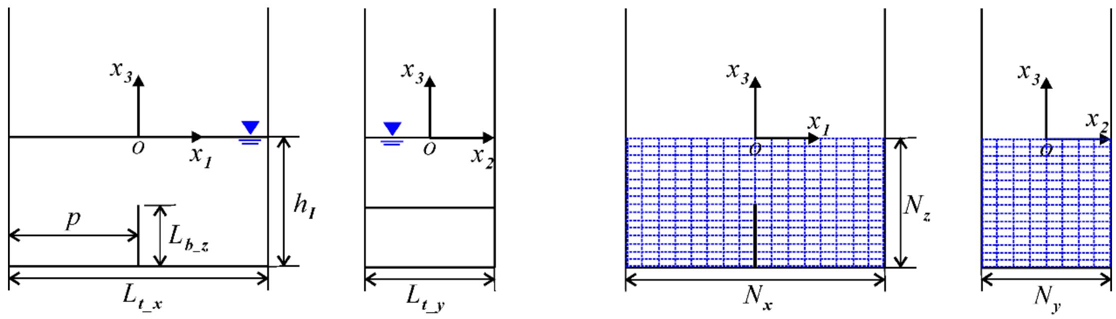

(a) (b)

Fig. 2 A three dimensional rectangular tank ($h_I / L_{t\_x} = 0.5$, $L_{t\_x} / L_{t\_y} = 0.5$, $p / L_{t\_x} = 0.5$): (a) geometry, and (b) finite element discretization ($N_x = N_z = 16$, $N_y = 8$)

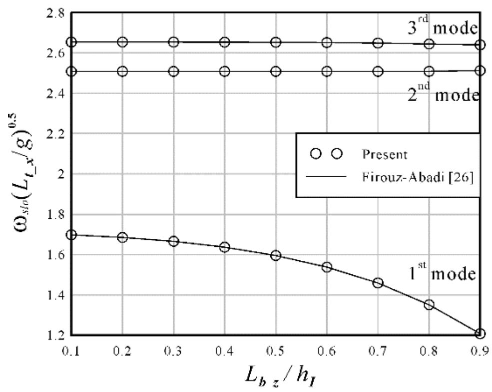

Fig. 3 Variation of dimensionless sloshing frequencies $\omega_{slo}\left(L_{t\_x} / g\right)^{0.5}$ in baffled tank

4.1 Natural sloshing frequency in baffled ARTs

The geometry of three dimensional rectangular tank with a bottom mounted vertical baffle is shown in Fig. 2(a) and the FE discretization of internal liquid is depicted in Fig. 2(b). Then, in Fig. 3, variation of the dimensionless sloshing frequencies obtained by Eq. (18) is compared with the results obtained by Firouz-Abadi *et al.* (2008). As depicted, the first three natural sloshing frequencies are in good agreements. Therefore, the proposed FE sloshing model is appropriate for the calculation of natural sloshing frequency in baffled tank and this model can be used for the hydrodynamic analysis of floating structures with baffled ARTs.

4.2 Hydrodynamic damping estimation

In this section, the numerical method for hydrodynamic damping estimation is verified by comparing with the previous numerical and experimental results (Goudarzi and Sabbagh-Yazdi 2012). Since the previous study was conducted under the lateral harmonic excitation, the present formulation should be modified by imposing the body boundary condition defined as

$$\frac{\partial \varphi_I}{\partial n} = j\omega X_0 n_i , \tag{24}$$

where X_0 is the horizontal displacement amplitude of the lateral motion.

Then, the corresponding weak form of internal fluid under the lateral harmonic excitation can be obtained without artificial free-surface damping

$$\begin{aligned} &\int_{{}^0S_{FI}} \rho_I \left(\frac{\omega^2}{g}\right) \varphi_I \overline{\varphi} \mathrm{d}S - \int_{{}^0V_{FI}} \rho_I \frac{\partial \varphi_I}{\partial x_i} \frac{\partial \overline{\varphi}}{\partial x_i} \mathrm{d}V \\ &= \int_{{}^0S_{WI}} j\omega \rho_I \; X_0 n_i \overline{\varphi} \mathrm{d}S. \end{aligned} \tag{25}$$

Finally, Eq. (25) can be expressed in the following discrete form

$$\left[\omega^2 \mathbf{F}_M^I - \mathbf{F}_K^I\right] \hat{\varphi}_I = j\omega \mathbf{R}$$

$$\text{with} \quad \mathbf{R} = \int_{{}^0S_{WI}} \rho_I X_0 n_i \mathrm{d}S . \tag{26}$$

As shown in Fig. 4(a), the same tank dimensions and loading conditions in reference results (Goudarzi and Sabbagh-Yazdi 2012) are used in collaborate with FE discretization shown in Fig. 2(b). In particular, among the various test cases, the single baffle located at the center of tank is only considered for comparison. Then, numerical tests are carried out for various aspect ratios (h_I / L_{t_x}) from 0.2 to 0.5 by solving the Eq. (26) to obtain the internal potential $\hat{\varphi}_I$. Finally, the corresponding sloshing damping ratio μ_{add} can be obtained through the Eqs. (19)-(23). The comparisons between reference results (Goudarzi and Sabbagh-Yazdi 2012) and present results are plotted in Fig. 4(b) with good agreements. Therefore, the approach that proposed in Section 3.3 is verified and can be extended to the numerical estimation of baffle induced hydrodynamic damping under the wave exciting loads.

4.3 Hydrodynamic code verification

The rigid body hydrodynamic analyses in “without ART” and “un-baffled ART” cases are implemented and verified through the comparison with WAMIT (Lee and Newman 2006). As shown in Fig. 5, a simple three dimensional box barge model is used for hydrodynamic

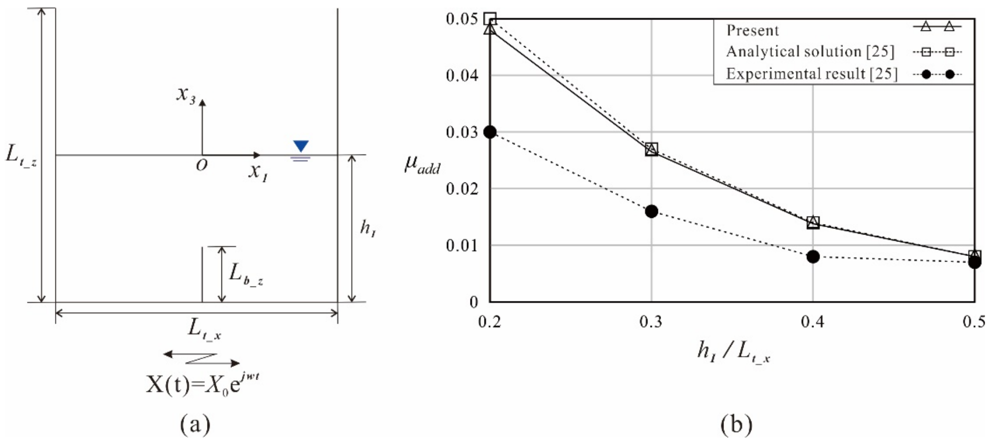

Fig. 4(a) A three dimensional rectangular tank ($L_{t\_x} = 96cm$, $L_{t\_y} = 40cm$, $L_{t\_z} = 100cm$ and $L_{b\_z} = 8cm$) with lateral harmonic excitation ($X(t) = X_0 e^{j\omega t}$ with $X_0 = 0.15cm$) and (b) Comparison of sloshing damping ratio μ_{add}

code comparison. At the center of barge, three rectangular free surface ARTs are located and all tanks are designed to be the same for simplicity. Then, the BMVB (bottom mounted vertical baffles) are installed at the center of tanks in x_2 direction. Note that the sloshing modeling in WAMIT is limited to the un-baffled ART case, the length of baffle is set to be zero ($L_{b\_z} = 0$) in this verification. The general information of box barge and the ARTs are summarized in Table 2 and its FE-BE discretization is listed in Table 3.

Then, the numerical implementation is performed by increasing the angular frequency ω from 0.2 to 0.8 rad/sec and by considering the two heading angles ($\theta = 45°$ and $\theta = 90°$). The density of the internal fluid ρ_I is 1000 kg/m^3, the density of the external fluid ρ_E is 1000kg/m^3, the depth h_E is assumed as infinite, and the gravitational acceleration g is set to be 9.8m/sec^2. In "un-baffled ART" case, the natural sloshing frequency is tuned to the natural roll frequency $\omega_{n,44}$ of barge by using the Eq. (17) and the artificial roll damping $\mathbf{S}_{C,44}$ and the free surface damping μ are set to zero.

In WAMIT, a higher-order method (4th-order B-spline functions) is employed to the external and internal fluids. Then, 60, 20, and 4 panels are used for the discretization of box barge and 18, 20, and 4 panels are used for each of the three ARTs in the length, width, and depth directions. Finally, the roll RAOs $A_{44}(\omega)$ in "without ART" and "un-baffled ART" cases is showed in Fig. 6 and good agreements are observed for both heading angles.

5. Numerical examples

This section describes the effects of natural sloshing frequency tuning and baffle ratio in baffled ARTs on the global roll motion of floating structure by investigating the maximum roll RAO and significant roll angle. Then, the hydrodynamic analysis of "baffle ART" are implemented by considering four natural sloshing frequency turning cases ("un-tuned", "tuned", "5% over-tuned", and "10% over-tuned") and five baffle ratios ($r_b = L_{b\_z} / L_{t\_z}$; r_b =0, 0.05, 0.10, 0.20, and 0.25). Finally, the results are compared with the hydrodynamic analysis of "without ART" and "un-baffled ART" cases to emphasize the effects of natural frequency tuning and baffle ratios in baffled ARTs.

In all hydrodynamic analyses, a simple three-dimensional box barge model that used in Section 4.3 is considered again. Then, the numerical implementation is performed by increasing the angular frequency ω from 0.2 to 1.2 rad/sec and one wave heading angle ($\theta = 90°$) is

Table 2 Information of 3D box barge, 3 tanks and baffle (filling ratio = 0.0 %)

3D box barge			
L_x (m)	300	I_{xx} ($kg \cdot m^2$)	7.60735E10
L_y (m)	50	I_{yy} ($kg \cdot m^2$)	1.28255E12
L_z (m)	30	I_{zz} ($kg \cdot m^2$)	1.32865E12
d (m)	10	COG(m)	(0,0,-0.91538)
Displacement (ton)	150000	$\omega_{n,44}$ (rad / sec)	0.487
ARTs		Baffle	
L_{t_x} (m)	4	L_{b_x} (m)	4
L_{t_y} (m)	40	L_{b_y} (m)	0 ~ 2.5
L_{t_z} (m)	10	t_b (m)	0.05

Table 3 Number of elements (N_x, N_y, and N_z) used in x_1, x_2, and x_3 directions

	N_x	N_y	N_z
Box barge	60	20	5 (4)*
Internal fluid (each tank)	4	40	8
External fluid	60	20	4

*The number of elements used for bottom to draft line is 4.

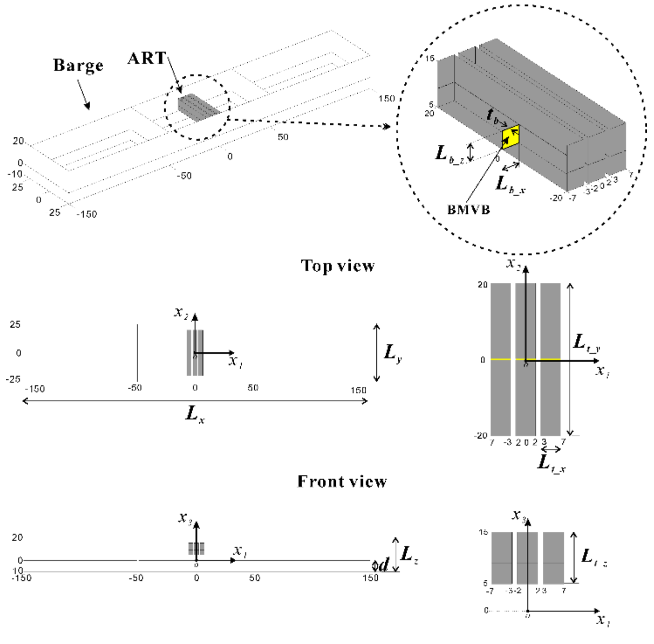

Fig. 5 Numerical example: (a) A three-dimensional box barge and (b) baffled ARTs

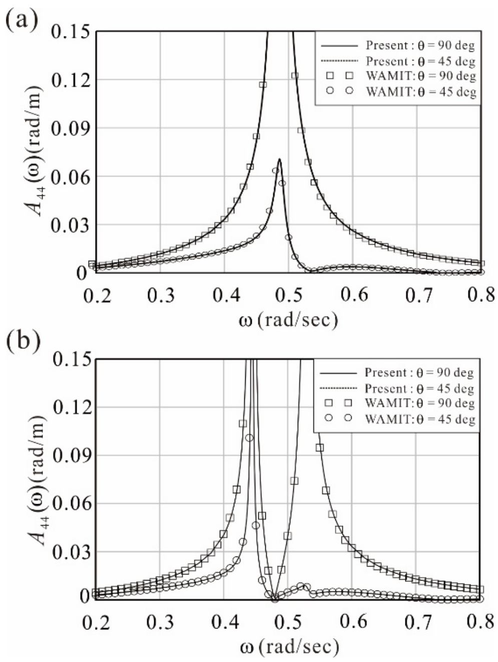

Fig. 6 Roll RAO $A_{44}(\omega)$ in (a) "Without ART" case and (b) "un-baffled ART" case

considered with 5% the artificial roll damping $\mathbf{S}_{C,44}$. In particular, the 1% initial tank damping $\mu_{initial}$ is used for the hydrodynamic analysis of "un-baffled ART" whereas the additional hydrodynamic damping $\mu_{add}(\omega)$ is added to initial tank damping $\mu_{initial}$ in "baffled ART" case. Note that the initial tank damping is used to avoid the improper resonance.

In advance to hydrodynamic analyses, the natural sloshing frequencies and the corresponding water depths should be obtained according to various tuning cases and

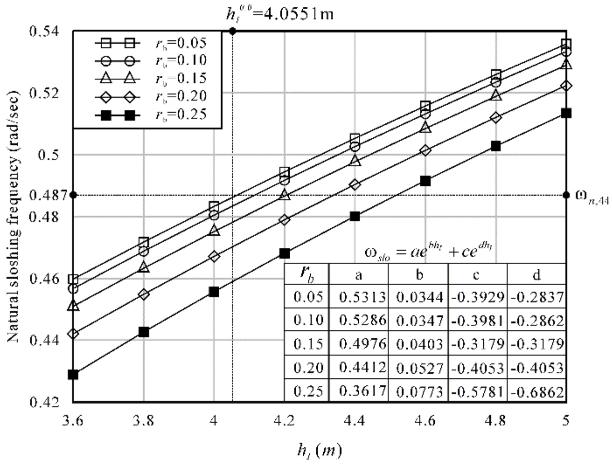

Fig. 7 Natural sloshing frequency curves by exponential fitting

Table 4 Natural sloshing frequency (ω_{slo}) and water depth ($h_I^{r_b}$) in baffled ARTs

r_b	Un-tuned	Tuned	Over-tuned	
			(5%)	(10%)
	$\omega_{slo} \neq \omega_{n,44}$	$\omega_{slo} \approx \omega_{n,44}$	$\omega_{slo} \approx 1.05\omega_{n,44}$	$\omega_{slo} \approx 1.10\omega_{n,44}$
	$h_I^{0.0}$	$h_I \neq h_I^{0.0}$	$h_I \neq h_I^{0.0}$	$h_I \neq h_I^{0.0}$
	$\omega_{slo}(rad/s)$	$h_I(m)$	$h_I(m)$	$h_I(m)$
0.05	0.486	4.0652	4.5145	4.9971
0.10	0.484	4.1166	4.5641	5.0467
0.15	0.478	4.2057	4.6538	5.1349
0.20	0.471	4.3398	4.7848	5.2613
0.25	0.459	4.5198	4.9564	5.4149

baffle ratios. Also, the hydrodynamic damping should be estimated under the wave exciting loads. Therefore, these two numerical procedures are introduced in followings.

5.1 Natural sloshing frequency tuning and hydrodynamic damping estimation

In this section, numerical procedures for natural sloshing frequency tuning and hydrodynamic damping estimation are demonstrated for the hydrodynamic analysis of floating structure with baffled ART. As mentioned, all values are evaluated with respect to four tuning cases and five baffle ratios.

5.1.1 Natural frequency tuning

Instead of using the analytic approach, the natural sloshing frequencies in baffled tanks are numerically evaluated by solving the discrete linear Eq. (18). Then, the series of numerical analyses are performed by changing the ratio of baffle r_b and the water depth h_I. Based on the results of numerical analyses, natural frequencies are approximated exponentially as shown in Fig. 7. Finally, in Table 4, the water depths for tuned and two over-tuned cases and the change of natural sloshing frequency for un-

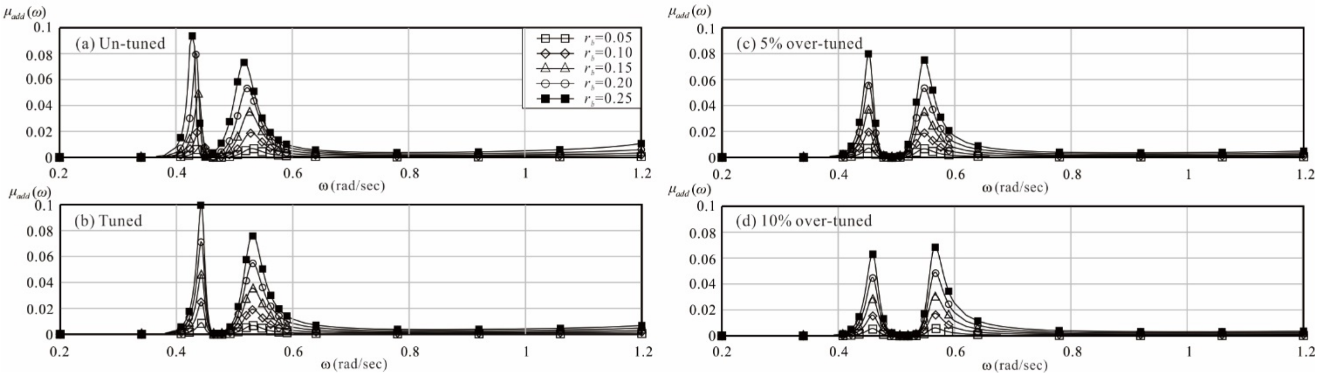

Fig. 8 Hydrodynamic damping $\mu_{add}(\omega)$: (a) un-tuned, (b) tuned, (c) 5% over-tuned, and (d) 10% over-tuned cases.

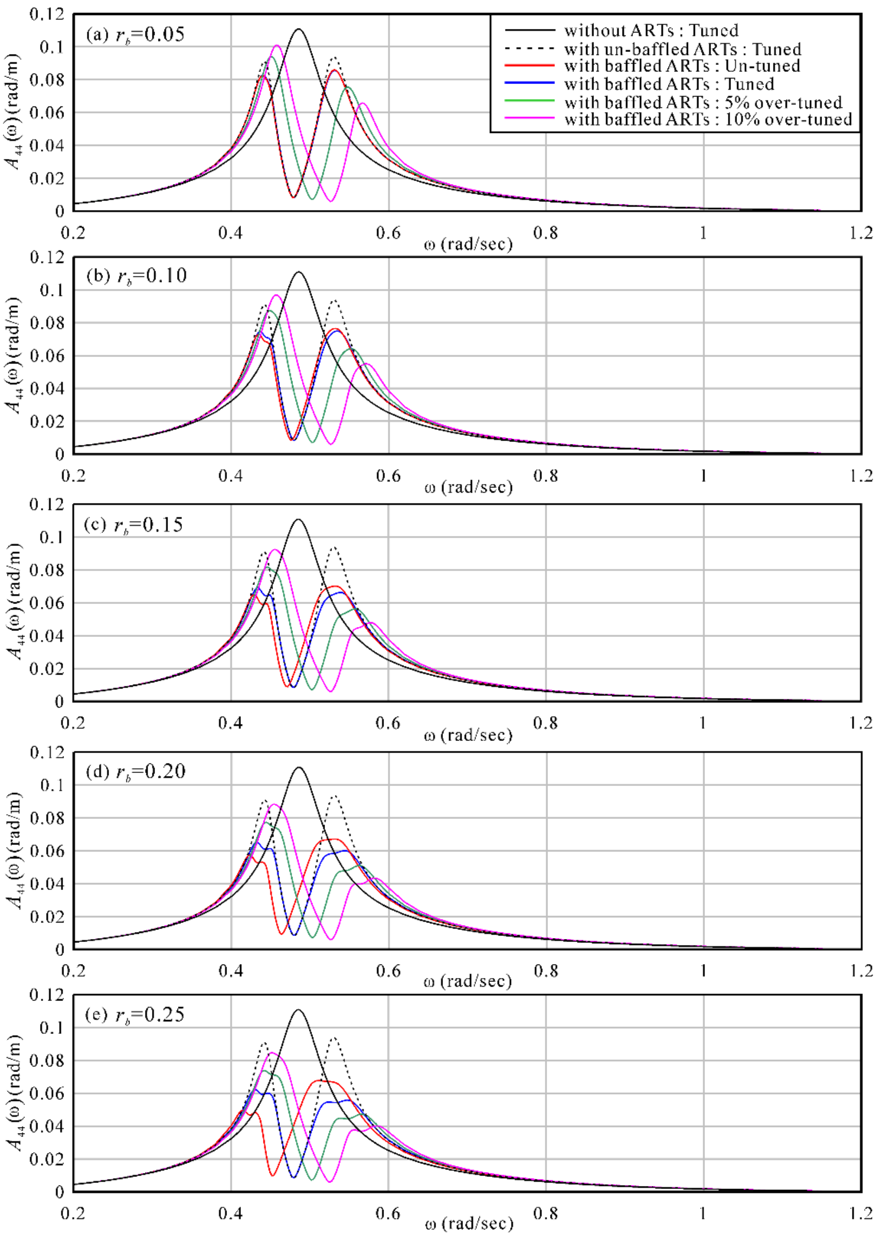

Fig. 9 Roll RAO $A_{44}(\omega)$ of various hydrodynamic analyses: (a) r_b =0.05, (b) r_b =0.10, (c) r_b =0.15, (d) r_b =0.20, and (e) r_b =0.25

tuned case are estimated through the fitted curves. It is shown that the natural sloshing frequency in tuned and two over-tuned cases can be set by increasing the water depth and the natural sloshing frequency of un-tuned case decrease without changing the water depth.

5.1.2 Hydrodynamic damping estimation

This section describes the numerical procedure for the estimation of additional hydrodynamic damping $\mu_{add}(\omega)$ under the wave exciting loads. The detail steps are followings;

• Implement the hydrodynamic analysis for "un-baffled ART" case to obtain the potential solution $\hat{\varphi}_I$ inside un-baffled tank.

• Evaluate the relative flow velocity V_f against to the baffle.

• Calculate the average rate of energy dissipation D and total energy of liquid E using the Eqs. (19)-(22).

• Estimate the additional hydrodynamic damping $\mu_{add}(\omega)$ using the Eq. (23).

As mentioned, the hydrodynamic analyses are implemented by varying the wave frequencies ω from 0.2 to 1.2 rad/sec with unit wave amplitude and 1% initial tank damping $\mu_{initial}$.

It should be note that the filling height h_I should be adjusted to make the natural sloshing frequency in un-baffled ART equals to natural sloshing frequency in baffled ART for various tuning cases. In un-baffled rectangular tank case, water depth h_I can be easily obtained using the Eq. (17), resulting in 4.0494 m, 4.0032 m, 3.9155 m, 3.7837 m, and 3.6012 m for five different natural sloshing frequencies of un-tuned case. Also, 4.0551 m, 4.5044 m, and 4.9876 m are used for the hydrodynamic damping estimation in tuned, 5% over-tuned, and 10% over-tuned cases, respectively.

Then, in Fig. 8, the hydrodynamic damping $\mu_{add}(\omega)$ is estimated against to four natural frequency tuning cases (un-tuned, tuned, 5% over-tuned, 10% over-tuned) and five baffle ratios (r_b = 0.00, 0.05, 0.10, 0.20, and 0.25). It is shown that hydrodynamic damping $\mu_{add}(\omega)$ increase as the baffle ratio r_b increase and it varies with respect to wave frequencies.

5.2 Effects of natural frequency tuning and baffle ratio

The natural frequency tuning and baffle ratio are the most important parameter in preliminary design of free surface ARTs. In this section, the effects of these two parameters on the global roll motion of box barge are investigated under the regular and irregular waves. For those, the series of numerical tests are implemented with respect to various natural frequency tuning cases and baffle ratios by taking the baffle induced hydrodynamic damping into consideration for the hydrodynamic analysis of "baffled ARTs".

5.2.1 Effects on the maximum roll RAO in regular waves

In this section, the effects of natural frequency tuning and baffle ratio of baffled ART system on the maximum roll RAO $A_{\max,44}$ are discussed under the regular waves. Then, the maximum roll RAO $A_{\max,44}$ of "baffled ART" case is compared with the results of "without ART" and "un-baffled ART" cases to emphasize the effects of baffled ART system.

Table 5 Relation between the Beaufort wind scale and the characteristic data of the JONSWAP and Brestscneider wave spectrums (Journée and Massie 2001)

	JONSWAP			Brestscneider		
	$H_{1/3}$ (m)	T_1 (sec)	T_p (m)	$H_{1/3}$ (m)	T_1 (sec)	T_p (m)
1	0.50	3.50	4.20	1.10	5.80	7.52
2	0.65	3.80	4.56	1.20	5.90	7.65
3	0.80	4.20	5.04	1.40	6.00	7.78
4	1.10	4.60	5.52	1.70	6.10	7.91
5	1.65	5.10	6.11	2.15	6.50	8.42
6	2.50	5.70	6.83	2.90	7.20	9.33
7	3.60	6.70	8.03	3.75	7.80	10.11
8	4.85	7.90	9.47	4.90	8.40	10.89
9	6.10	8.80	10.55	6.10	9.00	11.66
10	7.45	9.50	11.39	7.45	9.60	12.44
11	8.70	10.00	11.99	8.70	10.10	13.09
12	10.25	10.50	12.59	10.25	10.50	13.61

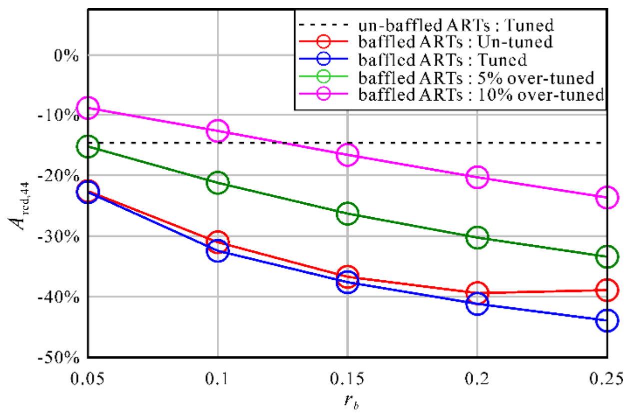

Fig. 10 Relative reduction of maximum roll RAO $A_{red,44}$

In Fig. 9, the roll RAO $A_{44}(\omega)$ is presented with respect to various tuning cases and baffle ratios. Also, the relative reduction of maximum roll RAO $A_{red,44}$ against to "without ART" are shown in Fig. 10. Then, the following remarks are observed:

• As shown in Fig. 10, in all tuning cases of "baffled ART", the reduction $A_{red,44}$ decrease as the baffle ratio r_b increase. This is because of the higher hydrodynamic damping ratio is obtained at higher baffle ratio. Also, the maximum reduction occurs in tuned case where the two peaks of roll RAO are well suppressed.

• In un-tuned cases, the reduction $A_{red,44}$ decrease as the baffle ratio r_b increase. But, when one or more baffles are devised in ARTs, this reduction will turn into increment in maximum roll RAO since the natural sloshing frequency is dramatically reduced without natural frequency tuning, resulting in unstable roll motion at higher frequency.

Table 6 Significant roll motion $A_{4,sig}^{(k)}$ for JONSWAP wave spectrum.

Sea state(k)	7		8		9		10	
	$A_{4,sig}^{(7)}$ (rad)	r (%)	$A_{4,sig}^{(8)}$ (rad)	r (%)	$A_{4,sig}^{(9)}$ (rad)	r (%)	$A_{4,sig}^{(10)}$ (rad)	r (%)
Without ART	0.0163		0.0527		0.1047		0.1720	
Un-baffled ART	0.0192	17.95	0.0564	7.03	0.1100	5.09	0.1765	2.64
Baffled ART	Un-tuned($\omega_{slo} \neq \omega_{n,44}$)							
r_b = 0.05	0.0189	16.38	0.0550	4.39	0.1068	1.95	0.1696	-1.41
0.10	0.0186	14.24	0.0532	1.05	0.1024	-2.19	0.1607	-6.56
0.15	0.0183	12.38	0.0519	-1.44	0.0990	-5.41	0.1542	-10.33
0.20	0.0181	11.01	0.0513	-2.71	0.0972	-7.18	0.1511	-12.15
0.25	0.0179	10.07	0.0513	-2.73	0.0970	-7.40	0.1513	-12.00
	Tuned($\omega_{slo} \approx \omega_{n,44}$)							
r_b = 0.05	0.0189	16.42	0.0550	4.33	0.1067	1.93	0.1694	-1.52
0.10	0.0186	14.33	0.0530	0.59	0.1021	-2.51	0.1592	-7.42
0.15	0.0183	12.56	0.0513	-2.66	0.0979	-6.47	0.1501	-12.71
0.20	0.0181	11.18	0.0500	-5.16	0.0946	-9.63	0.1429	-16.93
0.25	0.0179	10.14	0.0490	-7.01	0.0922	-11.95	0.1375	-20.03
	5% over-tuned($\omega_{slo} \approx 1.05\omega_{n,44}$)							
r_b = 0.05	0.0192	18.00	0.0540	2.47	0.1060	1.24	0.1588	-7.67
0.10	0.0187	15.01	0.0518	-1.77	0.1004	-4.09	0.1478	-14.03
0.15	0.0183	12.60	0.0499	-5.28	0.0956	-8.73	0.1385	-19.49
0.20	0.0180	10.81	0.0485	-7.92	0.0918	-12.37	0.1313	-23.66
0.25	0.0178	9.51	0.0475	-9.84	0.0889	-15.13	0.1260	-26.73
	10% over-tuned($\omega_{slo} \approx 1.10\omega_{n,44}$)							
r_b = 0.05	0.0193	18.88	0.0536	1.67	0.1048	0.10	0.1454	-15.45
0.10	0.0187	15.13	0.0513	-2.61	0.0987	-5.74	0.1364	-20.67
0.15	0.0182	12.03	0.0494	-6.24	0.0935	-10.76	0.1289	-25.06
0.20	0.0179	9.82	0.0480	-8.96	0.0893	-14.70	0.1230	-28.48
0.25	0.0176	8.29	0.0469	-11.06	0.0861	-17.75	0.1186	-31.03

*r (%) : relative reduction of significant roll motion against to "without ART" case

• If the natural sloshing frequency is over-tuned, the one of two peaks of roll RAO is relatively greater than other peak. Therefore, the performance of ART in over-tuned case couldn't surpass the tuned case. Therefore, the natural sloshing frequency should be tuned in terms of maximum roll reduction.

• Lastly, as the ratio of baffle r_b increase, the peak frequency is shifted to the higher wave frequency region in un-tuned case whereas it is shifted to lower wave frequency range in two over-tuned cases. These affect the performance of ARTs in irregular waves and those will be discussed in next section.

5.2.2 Effects on significant roll motion in irregular waves

This section describes the effects of baffled ARTs on the significant roll motion of barge in irregular waves. For the spectral analysis, the widely used wave energy spectrums are considered. Initially, the following Mean JONSWAP (Joint North Sea Wave Project) wave spectrum is considered as an irregular wave data in fetch limited situations

$$S_J^{(k)}(\omega) = \frac{320(H_{1/3})^2}{T_p^4}\omega^{-5}\exp\left(\frac{-1950}{T_p^4}\omega^{-4}\right)\gamma^{\lambda} \quad \text{with}$$
$$\lambda = \exp\left\{-\left(\frac{\omega/\omega_p - 1}{\sigma\sqrt{2}}\right)^2\right\}, \quad \omega_p = \frac{2\pi}{T_p} \quad \text{and} \tag{27}$$
$$\sigma = \begin{cases} 0.07; & \omega < \omega_p \\ 0.09; & \omega > \omega_p \end{cases},$$

where $H_{1/3}$ is the significant wave height, T_P and ω_P are the peak period and frequency at the spectral peak, and γ is the peakedness factor ($\gamma = 3.3$). In particular, the peak period T_P can be obtained through the relation with mean centroid wave period T_1

Table 7 Significant roll motion $A_{4,sig}^{(k)}$ for Brestschneider wave spectrum

Sea state(k)	7		8		9		10	
	$A_{4,sig}^{(7)}$ (rad)	r (%)	$A_{4,sig}^{(8)}$ (rad)	r (%)	$A_{4,sig}^{(9)}$ (rad)	r (%)	$A_{4,sig}^{(10)}$ (rad)	r (%)
Without ART	0.0590		0.0965		0.1384		0.1836	
Un-baffled ART	0.0571	-3.15	0.0881	-8.76	0.1224	-11.60	0.1602	-12.73
Baffled ART	Un-tuned($\omega_{slo} \neq \omega_{n,44}$)							
r_b = 0.05	0.0552	-6.50	0.0848	-12.17	0.1177	-15.01	0.1540	-16.12
0.10	0.0527	-10.69	0.0806	-16.48	0.1115	-19.44	0.1457	-20.62
0.15	0.0509	-13.64	0.0776	-19.61	0.1069	-22.78	0.1392	-24.16
0.20	0.0502	-14.82	0.0763	-20.91	0.1047	-24.36	0.1358	-26.04
0.25	0.0506	-14.14	0.0770	-20.18	0.1054	-23.85	0.1361	-25.87
	Tuned($\omega_{slo} \approx \omega_{n,44}$)							
r_b = 0.05	0.0551	-6.61	0.0847	-12.26	0.1176	-15.08	0.1539	-16.16
0.10	0.0522	-11.47	0.0800	-17.13	0.1109	-19.89	0.1452	-20.88
0.15	0.0497	-15.74	0.0759	-21.40	0.1051	-24.09	0.1377	-24.99
0.20	0.0477	-19.10	0.0727	-24.71	0.1006	-27.32	0.1319	-28.13
0.25	0.0463	-21.53	0.0704	-27.09	0.0974	-29.62	0.1279	-30.35
	5% over-tuned($\omega_{slo} \approx 1.05\omega_{n,44}$)							
r_b = 0.05	0.0527	-10.59	0.0820	-15.04	0.1156	-16.49	0.1534	-16.43
0.10	0.0498	-15.65	0.0774	-19.77	0.1095	-20.91	0.1458	-20.59
0.15	0.0472	-19.98	0.0735	-23.88	0.1041	-24.80	0.1390	-24.29
0.20	0.0452	-23.30	0.0704	-27.08	0.0999	-27.87	0.1336	-27.24
0.25	0.0438	-25.76	0.0681	-29.47	0.0966	-30.19	0.1294	-29.50
	10% over-tuned($\omega_{slo} \approx 1.10\omega_{n,44}$)							
r_b = 0.05	0.0513	-13.11	0.0812	-15.90	0.1163	-16.02	0.1559	-15.08
0.10	0.0486	-17.57	0.0775	-19.73	0.1116	-19.39	0.1503	-18.12
0.15	0.0464	-21.40	0.0742	-23.13	0.1074	-22.45	0.1451	-20.94
0.20	0.0446	-24.43	0.0715	-25.91	0.1038	-25.04	0.1406	-23.39
0.25	0.0432	-26.84	0.0693	-28.25	0.1006	-27.31	0.1366	-25.59

*r (%) : relative reduction of significant roll motion against to "without ART" case

$$T_p = 1.199 T_1 . \tag{28}$$

In addition, the Brestschneider wave spectrum which suited for open sea area is considered

$$S_B^{(k)}(\omega) = \frac{173\left(H_{1/3}\right)^2}{T_1^4}\omega^{-5}\exp\left(\frac{-692}{T_1^4}\omega^{-4}\right) \quad \text{with} \qquad T_p = 1.296 T_1 . \tag{29}$$

In Fig. 11, the JONSWAP wave spectrum $S_J^{(k)}$ and Brestschneider wave spectrums $S_B^{(k)}$ at sea state 7, 8, 9, and 10 are evaluated through the relation between the sea states defined by the Beaufort scale and the characteristic data of the wave spectrums listed in Table 5. Note that the peak frequency of Brestschneider wave spectrum is lower than JONSWAP wave spectrum at all sea states.

In followings, the conventional spectral analysis (Price and Bishop 1974, Journee and Massie 2001) is briefly addressed to obtain the significant roll motion of floating structures in irregular waves. Most of all, the roll RAO of box barge in regular waves should be found and the wave energy spectrums should be defined. Then, the relation between wave energy spectrum and the energy spectrum of floating structure is obtained at sea state k as followings

$$S_x^{(k)}(\omega) = \left|A_{44}(\omega)\right|^2 S_{\eta_a}^{(k)}(\omega) , \tag{30}$$

where $S_{\eta_a}^{(k)}(\omega)$ and $S_x^{(k)}(\omega)$ are energy spectrums for wave and motion of floating structure at sea state k, respectively.

Finally, the significant roll motion amplitude is defined by

$$A_{sig,44}^{(k)} = 2\sqrt{m_0^{(k)}} \quad \text{with} \qquad m_0^{(k)} = \int_0^\infty S_x^{(k)}(\omega)d\omega \tag{31}$$

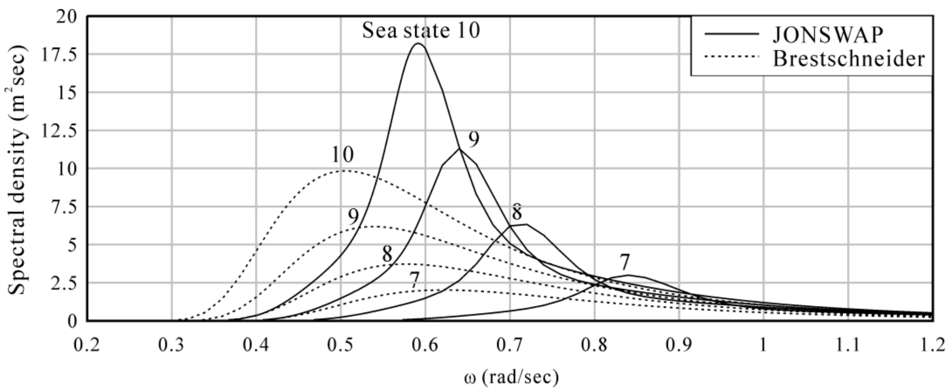

Fig. 11 Spectral density of JONSWAP and Brestschneider wave spectrums

in which $m_0^{(k)}$ is the zero order moment. Note that the zero order moment of motion energy spectrum $S_x^{(k)}(\omega)$ is integrated over the wave frequency from 0.2 to 1.2.

In Tables 6 and 7, the significant roll angles $A_{sig,44}^{(k)}$ for different sea states, wave spectrums, and hydrodynamic analysis cases are broadly calculated. In addition, the relative reduction of significant roll angle r against to "without ART" case is evaluated for the comparison. In followings, some remarks are described:

• As expected, higher significant roll motion is observed at higher sea state in all hydrodynamic analysis cases and the reduction of significant roll angle r is getting larger as the baffle ratio increase.

• In "un-baffled ART" case, the significant roll motion is not sufficiently reduced by ARTs since the roll RAO $A_{44}(\omega)$ is not reduced over the wide range of wave frequencies. In contrast, the significant roll motion of "baffled ART" case is well reduced in all tuning cases except un-tuned case. Therefore, in baffled ART case, the natural sloshing frequency should be tuned or over-tuned.

• In JONSWAP wave spectrum case, the significant roll motion is mostly suppressed in 10% over-tuned case. This is because the peak frequency of roll motion is getting away from the peak frequency of JONSWAP wave spectrum as the baffle ratio increased.

• When it comes to Brestschneider spectrum, the significant roll motion is not significantly affected by the natural frequency tuning since the wave energy is spread out at wide wave frequencies with small magnitude, resulting in sufficient reduction for tuned and two over-tuned cases as well as the un-tuned case.

6. Conclusions

In this study, numerical method for hydrodynamic analysis of floating structure with baffled ART was introduced in regular and irregular waves. For those, the direct coupled FEM-BEM formulation was developed through the linear potential theory and continuum mechanics to handle the coupled ship motion and sloshing problem with baffled ARTs as well as the arbitrary geometry. Moreover, the general capacity of 3D potential code was demonstrated through the estimation of natural sloshing frequency and hydrodynamic damping estimation in baffled ART.

In numerical examples, the proposed formulation was verified by comparing with numerical and experimental results. Then, the various hydrodynamic analyses and spectral analysis were conducted to emphasize the effects of natural sloshing frequency tuning and baffle ratio of baffled ART system on the roll motions. Finally, the following remarks have been made:

• In un-tuned and over-tuned cases, the ART system is no longer effective in reduction of maximum roll RAO whereas two peaks of roll RAO are well suppressed in tuned case.

• The significant roll angle is mostly affected by the distance between peak frequencies of roll RAO and wave spectrum. This means that the reduction of significant roll angle will not be significant when the peak frequency of sea spectrum and the roll natural frequency are getting closed.

• In all tuning cases, the maximum and significant roll motions were mostly suppressed in the biggest baffle ratio (r_b =0.25) since the hydrodynamic damping $\mathbf{F}_{\mathbf{C},add}^{\mathbf{I}}(\omega)$ increase as the baffle ratio r_b increase.

• Practically, the un-tuned and over-tuned cases can intentionally be considered to avoid the synchronization between peak frequencies of roll RAO and wave spectrum. However, the deep consideration is still required in context of maximum roll RAO.

In conclusion, effects of natural frequency tuning and baffle ratio should be taken into the preliminary design of baffled ART system as well as other considerations (i.e. location, size, mass of ARTs) since they affect the global roll motion significantly.

Acknowledgments

This research was supported by a grant (KCG-01-2017-01) through the Disaster and Safety Management Institute funded by Korea Coast Guard of Korean government. This work also was supported by "Human Resources Program in Energy Technology" of the Korea Institute of Energy Technology Evaluation and Planning (KETEP), granted financial resource from the Ministry of Trade, Industry & Energy, Republic of Korea (No.20184030202000).

References

Bhosale, A.D. and Murudi, M.M. (2017), "Seismic control of structures using sloped bottom tuned liquid dampers", *Struct. Eng. Mech.*, **64**(2), 233-241.

Bureau Veritas (2007), *Hydrostar for Experts User Manual*, Research Department Bureau Veritas Press, Paris, France.

Cho, J.R., Han, K.C., Hwang, S.W., Cho, C.S. and Lim, O.K. (2012), "Mobile harbor: structural dynamic response of RORI crane to wave-induced rolling excitation", *Struct. Eng. Mech.*, **43**(5), 679-690.

Faltinsen, O.M. and Timokha, A.N. (2009), *Sloshing*, Cambridge University Press.

Firouz□Abadi, R.D., Haddadpour, H., Noorian, M.A. and Ghasemi, M. (2008), "A 3D BEM model for liquid sloshing in baffled tanks", *Int. J. Numer. Meth. Eng.*, **76**(9), 1419-1433.

Francescutto, A. and Contento, G. (1999), "An investigation on the applicability of simplified mathematical models to the roll-sloshing problem", *Int. J. Offsh. Pol. Eng.*, **9**(2), 97-104.

Froude, W. (1861), "On the rolling of ships", *Trans. Inst. Nav. Archit.*, **2**, 180-227.

Goodrich, G.J. (1969), "Development and design of passive roll stabilisers", *Trans. Inst. Nav. Archit.*, **111**, 81-95.

Goudarzi, M.A. and Sabbagh-Yazdi, S.R. (2012), "Analytical and experimental evaluation on the effectiveness of upper mounted baffles with respect to commonly used baffles", *Ocean Eng.*, **42**, 205-217.

Iglesias, A.S., Rojas, L.P. and Rodríguez, R.Z. (2004), "Simulation of anti-roll tanks and sloshing type problems with smoothed particle hydrodynamics", *Ocean Eng.*, **31**(8-9), 1169-1192.

Isaacson, M. and Premasiri, S. (2001), "Hydrodynamic damping due to baffles in a rectangular tank", *Can. J. Civil Eng.*, **28**(4), 608-616.

Jeon, S.H., Seo, M.W., Cho, Y.U., Park, W.G. and Jeong, W.B. (2013), "Sloshing characteristics of an annular cylindrical tuned liquid damper for spar-type floating offshore wind turbine", *Struct. Eng. Mech.*, **47**(3), 331-343.

Journée, J.M. and Massie, W.W. (2001), *Offshore Hydrodynamics*, Delft University of Technology, Delft, the Netherlands.

Khabakhpasheva, T.I. and Korobkin, A.A. (2002), "Hydroelastic behaviour of compound floating plate in waves", *J. Eng. Math.*, **44**(1), 21-40.

Kim, K.T., Lee, P.S. and Park, K.C. (2013), "A direct coupling method for 3D hydroelastic analysis of floating structures", *Int. J. Numer. Meth. Eng.*, **96**(13), 842-866.

Kim, Y. (2002), "A numerical study on sloshing flows coupled with ship motion-the anti-rolling tank problem", *J. Ship Res.*, **46**(1), 52-62.

Lee, B.S. and Vassaols, D. (1996), "An investigation into the stabilisation effects of anti-roll tanks with flow obstructions", *Int. Shipbuil. Prog.*, **43**(433), 70-88.

Lee, C.H. and Newman, J.N. (2006), *WAMIT User Manual*, Department of Ocean Engineering, MIT, Cambridge, MA, U.S.A.

Lee, K.H. and Lee, P.S. (2016), "*Nonlinear hydrostatic analysis of flexible floating structures*", *Appl. Ocean Res.*, **59**, 165-182.

Lee, K.H., Cho, S., Kim, K.T., Kim, J.G. and Lee, P.S. (2015), "Hydroelastic analysis of floating structures with liquid tanks and comparison with experimental tests", *Appl. Ocean Res.*, **52**, 167-187.

Lewison, G.R.G. (1976), "Optimum design of passive roll stabilizer tanks", *Trans. Inst. Nav. Archit.*, 31-45.

Maleki, A. and Ziyaeifar, M. (2008), "Sloshing damping in cylindrical liquid storage tanks with baffles", *J. Sound Vibr.*, **311**(1-2), 372-385.

Miles, J.W. (1958), "Ring damping of free surface oscillations in a circular tank", *J. Appl. Mech.*, **25**(2), 274-276.

Moaleji, R. and Greig, A.R. (2007), "On the development of ship anti-roll tanks", *Ocean Eng.*, **34**(1), 103-121.

Price, W.G. and Bishop, R.E.D. (1974), *Probabilistic Theory of Ship Dynamics*, Chapman and Hall, London, U.K.

Rahman, M.S., Islam, M.S., Do, J. and Kim, D. (2017), "Response surface methodology based multi-objective optimization of tuned mass damper for jacket supported offshore wind turbine", *Struct. Eng. Mech.*, **63**(3), 303-315.

Sellars, F.H. and Martin, J.P. (1992), "Selection and evaluation of ship roll stabilization systems", *Mar. Technol.*, *SNAME*, **29**(2), 84-101.

Souto, A. and González, V. (2001), "Passive stabilizer tanks simulation using SPH models", *Proceedings of the Fluid Structure Interaction*, Halkidiki, Greece.

Taylor, R.E. (2007), "Hydroelastic analysis of plates and some approximations", *J. Eng. Math.*, **58**(1-4), 267-278.

Van Den Bosch, J.J. and Vugts, J.H. (1966), "On roll damping by free-surface tanks", *Trans. Inst. Nav. Archit.*

Wang, C.D. and Meylan, M.H. (2004), "A higher-order-coupled boundary element and finite element method for the wave forcing of a floating elastic plate", *J. Flu. Struct.*, **19**(4), 557-572.

Watts, P. (1883), "On a method of reducing the rolling of ships at sea", *Trans. Inst. Nav. Archit.*, **24**, 165-190.

Watts, P. (1885), "The use of water chambers for reducing the rolling of ships at sea", *Trans. Inst. Nav. Archit.*, **26**.

Yoon, J.S. and Lee, P.S. (2017), "Towards hydro-elastoplastic analysis of floating plate structures", *J. Flu. Struct.*, **71**, 164-182.

PL